Optical phonons, crystal-field transitions, and europium luminescence-excitation processes in Eu_2BaCoO_5: Experiment and theory

S. Taboada and A. de Andrés
Instituto de Ciencia de Materiales de Madrid, Consejo Superior de Investigaciones Científicas, Facultad de Ciencias C-4, Cantoblanco E-28049, Madrid, Spain

J.E. Muñoz Santiuste
Escuela Politécnica Superior, Universidad Carlos III de Madrid, Avenida del Mediterraneo 20, Leganés E-28913, Madrid, Spain

C. Prieto and J.L. Martínez
Instituto de Ciencia de Materiales de Madrid, Consejo Superior de Investigaciones Científicas, Facultad de Ciencias C-4, Cantoblanco E-28049, Madrid, Spain

A. Criado
Instituto de Ciencia de Materiales de Sevilla, Departamento de Física de la Materia Condensada, Universidad de Sevilla, Box 1065 E-41080, Spain
(Received 16 November 1993; revised manuscript received 13 May 1994)

The europium compound Eu_2BaCoO_5 has been studied by means of Raman and x-ray absorption spectroscopies. The eigenfunctions and frequencies of the optical normal modes have been calculated from an adequate potential showing good accordance with the observed phonons. In addition to Raman allowed normal modes, several infrared and luminescence bands are observed between 10 K and 300 K. The temperature dependence of these processes has allowed us to determine the complex interrelation between these two kinds of elementary excitations. A broad luminescence band (at 2.3 eV) is tentatively attributed to electronic transitions between Co^{2+} 3d crystal field levels in the gap of the material. The mixing of these quasiatomic levels with apical oxygen orbitals, along the very short Co-O(2) bonds in the chains, can be the reason for the simultaneous enhancement of the intensities of the luminescence band and of the apical oxygen infrared modes through a resonant electron-phonon coupling. From the dependence of the phonon frequencies and the analysis of the extended x-ray-absorption fine structure spectra with the temperature it can be concluded that on decreasing the temperature the a-axis becomes shorter, while the other two axes remain nearly unchanged. The emission spectrum in the visible range has been observed and interpreted in the frame of the crystal-field theory. We have studied the dependence of the intensity of the electronic transitions between $4f$ levels of the europium ions with the temperature and the energy of the exciting light. From the behavior of the Eu^{3+} luminescence peaks it has been possible to determine the processes of excitation and emission, which are shown to involve lattice phonons. The crystal-field parameters of the Eu^{3+} ions have been calculated from the energies of the lower terms of the ion.

I. INTRODUCTION

The compounds with R_2BaMO_5 formula, where R=rare earth, and M= transition metal, that crystalize in the *Immm* structure are attracting vast interest because of the peculiarities of this structure composed of isolated chains of MO_6 octahedra. Its simplicity makes the study of the related physical properties fascinating. Magnetic characterization of these nearly perfect one-dimensional (1D) Heisenberg antiferromagnets is being actively studied.[1,2]

Nickel oxides, with R=Nd to Yb, have been recently structurally described as belonging to the *Immm* space group.[1,2] This structure is also adopted by some Co oxides. The *Immm* structure consists of one-dimensional chains of Co-O octahedra. These octahedra are only connected by the apical oxygens called O(2) along the a axis, but the chains are not directly connected and the Co-Co distances are quite long so that the system can really be considered as 1D from the magnetic point of view. The octahedra present a strong tetrahedral deformation with very short Co-O(2) bonds (1.89 Å) and quite larger Co-in plane-O bonds (2.22 Å). In the case of the Ni compounds, the effect of the orbitals on the deformation of the Ni-O octahedra has been evaluated[3] from a semiempirical model.

Optical Raman phonons have been studied in compounds of the same family with different structures and the force constants were evaluated.[4,5] The compounds with the *Immm* structure present Raman spectra that agree with the group theory predictions, but a weak forbidden Raman peak, the IR-active stretching mode of the apical oxygen, is observed probably due to the presence of some defects, like small quantities of different rare-earth ions.

The study of the rare-earth crystal-field transitions by means of a very high resolution spectroscopic technique can give information on the magnetic order in the sample as has been done as a function of the temperature in nickelates[6] and cuprates[7] with R_2BaMO_5 composition. The coupling between a low-energy crystal-field transition and a phonon of similar energy has been observed by Raman spectroscopy and explained theoretically in the case of $NdBa_2Cu_3O_{7-x}$.[8]

The electronic structure, in related compounds, of the localized states and bands, has attracted enormous interest and several experimental approaches have been used. For example, in cuprates and nickelates, through optical conductivity and reflectivity[9–11] and infrared absorption,[12,13] peaks around 1.7–2 eV have been assigned to transitions between different kind of electronic levels [charge transfer (CT) gap, transitions from Cu localized states to band states, oxygen $2p$ intraband]. A recent study has also been done in insulating Co compounds ($Bi_2M_3Co_2O_{9+d}$),[14] where a broad infrared absorption is observed as in the conducting $3d$ transition metal oxides; the CT and/or $d-d$ excitations of Co are found to lie above 4 eV. Some features of the electronic structure, in this kind of compound, have been explained but the problem is far from being resolved. Still, the theoretical calculations, often, can explain not even the gap, so that much more information is still necessary even in these relatively simple oxides.

In this work we study the complex behavior of the Eu_2BaCoO_5 compound as a function of the temperature by Raman scattering and x-ray absorption in combination with different theoretical models. The Raman technique allows to observe phonons and some electronic transitions, as luminescence peaks or bands, too weak to be detected with another luminescence setup. The scheme of the results presented in this work is as follows: Section III is dedicated to the optical phonons. After the description of the model used to calculate the frequencies and the eigenvectors, we discuss the assignment of the observed one-phonon peaks to normal modes at the different temperatures. Afterwards, the processes which produce the appearance of multiphonons and luminescence bands are discussed. In Sec. V, the combination of Raman and extended x-ray-absorption fine structure (EXAFS) spectroscopies have made possible the determination of the variation of some particular interatomic distances with the temperature.

In Sec. VI we present the observed emission spectra of the europium ion, in the visible range, as a function of the temperature (between 10 and 300 K) and of the excitation energy of the incident laser beam. Because the state from which we observe most of the emission lines is a singlet, the spectra are not very complicated and a clear picture of the fundamental states can be obtained. A theoretical approach has been done in order to describe the crystal field acting on the Eu^{3+} ion. In a first step, we have calculated the crystal-field parameters based on a single point charge electrostatic model using the x-ray structural data of Eu_2BaCoO_5. The energy level fitting is done as a second step, by diagonalizing the interaction matrix of the $4f^6$ configuration taking into account the observed splitting of the ^7F levels.

II. EXPERIMENTAL DETAILS

The Eu_2BaCoO_5 compounds were prepared as polycrystalline samples mixing stoichiometric amounts of the high purity oxides Eu_2O_3 (99.999%), CoO (99.99%), and $BaCO_3$ (99.999%). The homogenized mixture was heated at 950 °C for 12 h; then it was regrounded and reheated at 1050 °C for another 12 h. The heating treatment was done in argon flow due to the high instability of Co^{2+} ions in air at the high temperatures necessary to prepare these compounds.

Raman-scattering experiments have been performed with an $X-Y$ Dilor multichannel spectrometer using a Spectra Physics Ar^+ laser as excitation source with less than 10 mW on the samples, which were always in helium atmosphere, inside the chamber of an Oxford cryostat, in order to avoid heating damage. The luminescence of the samples was excited with the 476.5, 488, and 514.5 nm lines of the Ar^+ laser. The spectra were recorded between 300 K and 9 K in the available experimental spectral range (21 000–13 000 cm^{-1}). The apparatus response is strongly dependent on the frequency of the detected light in a such wide energy range, so that we have corrected all the spectra by the experimental set-up sensitivity.

The x-ray-diffraction data show that the samples are single phase and present the *Immm* structure. The structure has been checked only at room temperature (RT) with x-ray diffraction. Nevertheless, the *Immm* structure presented by these compounds is very stable and does not admit oxygen defects, and so no structural changes are expected when the temperature is varied.

The EXAFS experiments were carried out on the XAS-3 beam line at the DCI storage ring (Orsay, France) with an electron beam energy of 1.85 GeV and an average current of 250 mA. Data were collected with a fixed exit monochromator using two Si(311) crystals in transmission mode. Detection was made by using two ion chambers filled with air. The energy resolution was estimated to be better than 2 eV based on the Cu foil $3d$ near-edge feature. The energy calibration was monitored using the Cu foil sample, and was set as 8991 eV at the first maximum above the edge. Samples were prepared by grinding, sieving, and then selecting particles less than 10 μm in size by floating the powder. The particles were then spread on a tape. Several layers of tape were used to fabricate samples with an adequate absorption jump ($0.1 \leq \Delta\mu x \leq 1.0$) and a maximum for the total absorption of less than 1.5 ($\mu x \leq 1.5$).

III. OPTICAL PHONONS

The $Immm$ space group is orthorhombic with the D_{2h} point group ($Z = 1$ in the primitive cell). The factor group analysis of the $Immm$ structure[4] gives that 9 even modes are Raman active ($3A_g+1B_{1g}+2B_{2g}+3B_{3g}$) and 14 odd modes are infrared active ($5B_{1u}+5B_{2u}+4B_{3u}$). In this highly symmetric structure only Eu and O(1) can contribute to Raman modes. The apical oxygens O(2), which catenate the successive octahedra, can contribute, in principle, only to infrared modes. Among the Raman modes, two of them (those with the lowest energies) correspond to Eu motions, five to the oxygens O(1), which form the basal planes of the Co-O octahedra, and the two modes left involve the two kinds of ions. These last two modes are not observed in our Raman spectra. The infrared (IR) modes involve always several kinds of ions, but it is possible to say that the higher-frequency ones (over 400 cm^{-1}) are basically due to motions of oxygen [O(1) and O(2)] and cobalt ions.

A. Lattice dynamics calculation

Crystal lattice modes have been calculated using the Born–von Karmán formalism,[15] in which the dynamical matrix is set up in terms of Cartesian force constants

$$\Phi_{\alpha\beta}(lk,l'k') = \frac{\partial^2 V}{\partial u_\alpha(lk)\partial u_\beta(l'k')} ,$$

where the force constant relating atomic displacements along α and β ($\alpha, \beta = x,y,z$) of atoms k and k' belonging to unit cells l and l' can be obtained as the second derivative of the crystal energy with respect to these displacements. The dynamical matrix can be obtained from these force constants as

$$D(\mathbf{q}|kk')(m_k\ m'_k)^{-1/2}\sum_{l'}\Phi(0k,lk') \times \exp\{i\mathbf{q}[\mathbf{r}(l'k') - \mathbf{r}(0k)]\} ,$$

where $\mathbf{q}$ is the wave vector and $\mathbf{r}(lk)$ and m_k are the position vector and mass of atom (lk), respectively. When Coulombic long-range forces are present, the sum over all unit cells l' converges very slowly and it is necessary to accelerate the convergence using the Ewald method.[16]

In order to be able to build up the dynamical matrix we need a model for the crystal lattice energy. In the case of ionic crystals, the equilibrium structure can be viewed as a compromise between the Coulombic attractive forces and the short-range repulsive forces arising from the overlapping of atomic orbitals. We have modeled the Coulombic forces considering for each ion its formal charge in the empirical formula whereas for the short-range forces, several parametrizations are available in the literature. We have chosen that proposed by Gilbert,[17] where the repulsion between two ions i and j can be expressed as

$$V_{ij}(\text{rep}) = f_0(B_i + B_j)\exp[(A_i + A_j - r_{ij})/(B_i + B_j)] .$$

Here, A and B are characteristic constants of the chemical kind of the ions involved and r_{ij} is the distance between them. The values of the A and B constants for barium, cobalt, and oxygen atoms have been taken from the literature.[18] For europium, no available data could be found and we proceeded to a determination of the A and B parameters. A least-squares refinement of these parameters was carried out in order to get an energy-minimized crystal configuration as close as possible to the experimental one. The minimization was performed with respect to the lattice parameters and the atomic positions maintaining the constraints of the $Immm$ crystal symmetry. For the optimized A and B parameters we found a discrepancy of 1.5%, 0.1% and 0.7% between minimized and experimental a, b and c lattice parameters, whereas the maximum atomic shift was 0.07 Å during the minimization process starting from the experimental structure. In Table I we show the final values of the parameter adopted in this work.

Using this potential model derived from static considerations, we have calculated the lattice dynamics at $q = 0$ by diagonalization of the dynamical matrix for $q = 0$. Our approach is within the rigid-ion model which deals the ions as rigid units, which precludes atomic polarization effects. The inclusion of such effects would require much more sophisticated approaches such as shell models. An alternative approach which retains the simplicity of the rigid-ion model considers effective Coulombic charges which account for polarization effects. The effective charge values are lower than the formal charge ones, modelling in this way the Coulombic screening because of polarization. The use of effective charges has been successfully applied to ionic materials such as $KNbO_3$ Ref. 19 and $YBa_2Cu_3O_7$.[20] In our case, the calculation of the Raman frequencies using the parameter values of Table I gave too large frequencies and we had to scale the free-ion charge values with a factor of 0.71 in order to get effective charges showing the best agreement between experimental and calculated frequencies. In order to keep the balance between Coulombic and repulsive forces, the V_{ij}(rep) terms were scaled accordingly with a factor of 0.51. Table II collects the phonons observed by Raman spectroscopy at room and low temperatures together with the calculated frequencies.

B. One-phonon processes

Figure 1 shows the Raman spectra obtained at different temperatures between 9 K and 300 K. The room

TABLE I. Static crystal energy parameters $V(r_{ij}) = Z_iZ_je^2/r_{ij} + f_0(B_i + B_j)\exp[(A_i + A_j - r_{ij})/(B_i + B_j)]$ with $f_0 = 1$ kcal mol^{-1} $Å^{-1}$. A factor of 0.51 was applied to this function in order to calculate the lattice frequencies.

Ion	A (Å)	B (Å)	Z
Eu	1.733	0.0959	+3
Ba	1.953	0.101	+2
Co	1.285	0.066	+2
O	1.853	0.168	-2

TABLE II. Calculated and observed optical phonon frequencies (in cm^{-1}); upper part, even modes, and lower part, odd modes. The phonons have been observed by Raman scattering at temperatures between 300 K and 10 K.

Species	Kind of ion involved in the motion	Calculated normal modes	Observed phonons 300 K	Observed phonons 10 K
B_{2g}	Eu	118	118	121
A_g	Eu	171	168	172
B_{3g}	Eu+O(1)	174		
B_{3g}	Eu+O(1)	181		
B_{1g}	O(1)	306		302
B_{2g}	O(1)	356		342
B_{3g}	O(1)	410	412	411
A_g	O(1)	445		
A_g	O(1)	550	508	508
B_{2u}		54		
B_{3u}		61		
B_{1u}		86		
B_{2u}		114		
B_{3u}		161		
B_{2u}		184		
B_{1u}		189		
A_u		221		(silent)
B_{2u}		288		270
B_{1u}		304		
B_{3u}		315		
B_{1u}		436		446
B_{2u}		436		446
B_{1u}		602		
B_{3u}		709	708	724

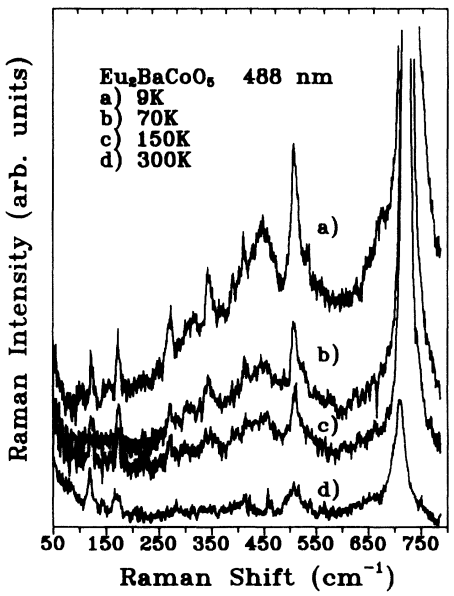

FIG. 1. One-phonon region of the Eu_2BaCoO_5 Raman spectra at different temperatures between 300 K and 9 K with the 488 nm excitation laser line. The 300 K spectrum is equivalent to the one of Ref. 5.

temperature spectra of isomorphous nickelates have been studied in previous works.[4,5] The very different atomic masses of the yttrium and the rare-earth ions (Ho, Er, and Tm) have already allowed us to observe, very clearly, the correct dependence of the frequency with the lanthanide mass in the first two observed peaks showing that they correspond exclusively to movements of R ions. The remaining observed peaks are only related to oxygen motions. These two conclusions are now checked by the calculations of the normal mode eigenvectors and frequencies. The peak at 708 cm^{-1}, which is observed around 740 cm^{-1} as a weak shoulder in other studied nickelates,[4] is the most important peak in the spectrum of Eu_2BaCoO_5 [Fig. 1(d)]. We assign this peak to the B_{3u} infrared M-O(2) stretching mode. The Co-O(2) distance is very short (around 1.89 Å), and so the frequency corresponding to its stretching is expected to be the highest of the one-phonon peaks.

When the temperature decreases, several changes are observed in the one-phonon region (below 750 cm^{-1}): (i) Some new peaks appear (their frequencies are compiled in Table II). (ii) The intensity of the infrared mode at 708 cm^{-1} shows a strong increase and the relative intensity of the remaining peaks also changes. (iii) The frequencies of the observed peaks vary in two different ways: The R ion modes and the 708 cm^{-1} peak increase around 2%, while the O(1) peaks remain unchanged or even decrease slightly. The calculation of the optical phonons has been done to obtain the eigenvectors and frequencies of the Raman- and infrared-active modes in order to compare them with the observed phonons. Table II collects the observed phonons by Raman spectroscopy at room and low (10 K) temperatures together with the calculated frequencies.

The so large intensity of the Raman-forbidden 708 cm^{-1} peak in the Eu compound can be produced by some kind of disorder in the structure. For example, the presence of different rare-earth ions as an impurity would break the inversion symmetry of the apical oxygens and transform this mode into a Raman-allowed one. Another possibility is that the structure is not correctly described by the *Immm* group but by some less symmetric group or that some kind of local distortion is present. Nevertheless, we have rescued these possibilities because (1) the x-ray diffraction spectra at room temperature are clearly indexed in the *Immm* group, (2) the structure is very stable, and (3) the oxides employed in the sample preparation are extremly pure. Another argument is that, with the only exception of the 708 cm^{-1} peak, the number and the frequencies of the Raman peaks, at room temperature, correspond to those expected from group theory.

It is known that cobalt oxide compounds are unstable when heated in air. We have performed Raman spectra with the sample in air, instead of the usual helium atmosphere, and have obtained that, actually, the heating produced by the 10 mW laser is enough to locally damage the sample. Nevertheless, the obtained spectrum (Fig. 2) contains none of the previously reported peaks (Fig. 1).

Another possibility, which we think is the correct one, is that the incident or scattered energies can be in resonance with some electronic transition which induces,

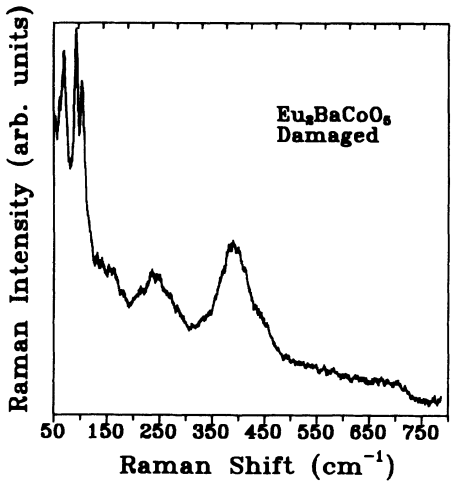

FIG. 2. Raman spectrum of an Eu_2BaCoO_5 sample damaged by the reaction of the hot spot zone with air.

through electron-phonon Fröhlich interaction, the Raman activity for the LO odd phonons. This is supported by the presence of the second, third, and even fourth order of this phonon marked in Fig. 3. Note that the intensity is clearly vanishing with the increasing order of the phonon.

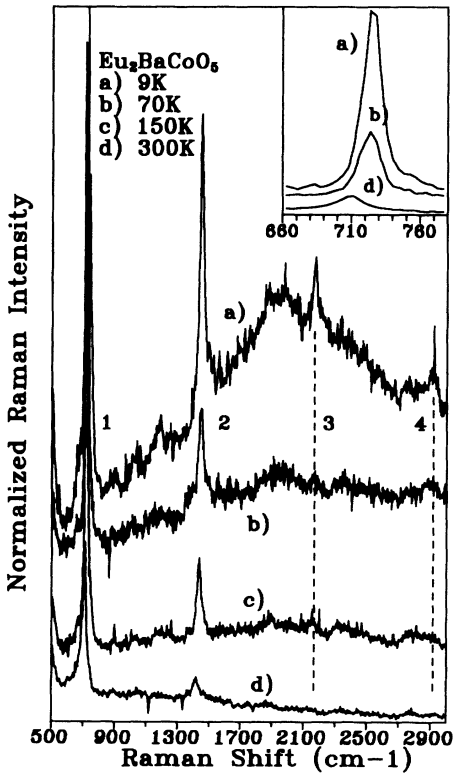

FIG. 3. Raman spectra of Eu_2BaCoO_5 showing the evolution of the intensity and frequency of the multiphonons with temperature. The excitation wavelength is 488 nm. The inset shows the enhancement of the B_{3u} phonon as the temperature decreases. Labels 1–4 indicate the order of the B_{3u} phonon.

On the other hand, the peaks observed in Fig. 1 when the temperature decreases can have several origins. The possibility of a structural phase transition which would induce the observation of new Raman-active phonons is disregarded because of the previously mentioned stability of the structure. Moreover, neutron-diffraction studies between RT and 1.5 K on the isostructural nickelates show that no structural phase transition happens in this system.

We rather propose that these new peaks have these two origins: Two peaks (at 302 and 342 cm^{-1}) are Raman modes not observed at RT whose intensities increase when the temperature is low enough, and the other ones (at 270 and 446 cm^{-1}) are infrared modes (as the 708 cm^{-1} one), forbidden but observed by Raman scattering. The two first mentioned peaks are detected in nickelates with the same structure at room temperature, probably because the scattering efficiency for all modes is higher. The 446 cm^{-1} peak is wider than the other phonons, probably because it comes from two infrared modes ($1B_{1u}$ and 1 B_{2u}; see Table II) whose calculated frequencies are identical, but could be slightly different, producing the observed broadening. These two infrared modes (270 and 446 cm^{-1}) involve basically Co-O(2) bond bending together with Co-O(1) bond bending and/or stretching, respectively. The highest-energy B_{3u} mode is principally due to the Co-O(2) bond stretching, and so it is clear that on lowering the temperature the infrared phonons that involve principally the Co-O(2) bonds are those that appear in the Raman spectra.

IV. INTERACTION BETWEEN PHONONS AND LUMINESCENCE PROCESSES

Figure 3 shows the spectra recorded at temperatures between 300 K and 9 K using the 488 nm laser line as excitation in the range between 500 and 3000 cm^{-1} where the multiphonons are observed. The frequencies of the peaks in the lowest-temperature spectrum are 724, 1448, 2170, and around 2910 cm^{-1}, which correspond to the first, second, third, and fourth order of the B_{3u} phonon, respectively. The shift in the energy of the first- and second-order peaks can be followed in all the temperature range from 708 to 724 cm^{-1} and from 1417 to 1448 cm^{-1}, respectively, showing a consistent variation. This figure clearly shows how the intensity of the B_{3u} peak and its multiples increases when the temperature decreases. Note that the "background" also changes considerably. The inset of Fig. 3 presents the evolution of the intensity and the frequency of the 708 cm^{-1} mode.

The spectra at low temperature for two incident wavelengths (476.5 and 488 nm) are shown in Fig. 4. The broadband corresponds to a luminescence process. Note that the phonon peaks are observed at the same position in the "Raman shift," while the luminescence peaks and band (marked with an arrow), where the absolute position in energy must be preserved, are observed with a shift equal to the separation between the two incident beam energies ($\Delta\omega_0$= 494 cm^{-1}, in the present case). This broadband, observed in the 476.5 nm (20986 cm^{-1}),

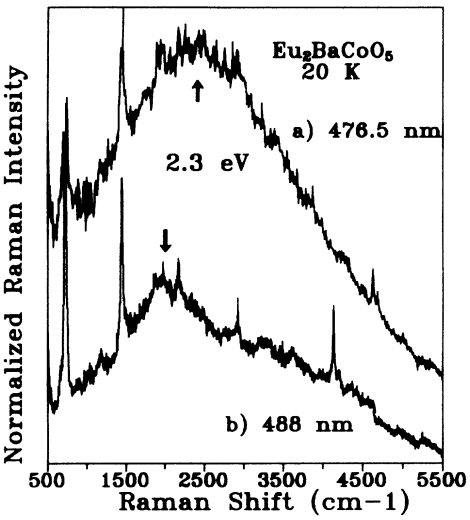

FIG. 4. Spectra of Eu_2BaCoO_5 at 20 K for the 488 and 476.5 nm excitation wavelengths showing the broad luminescence-type band, which corresponds to an absolute energy of 2.3 eV.

spectrum around a Raman shift of 2400 cm^{-1}, corresponds to an absolute energy of (20 986−2400 cm^{-1}=) 18586 cm^{-1} (= 2.32 eV).

The sharp luminescence peaks correspond to crystal-field transitions between the $4f$ levels localized in the Eu ions. These peaks are very sharp as it corresponds to emissions between these kinds of electronic levels. The assignment of the observed peaks and the calculation from two different models of the crystal-field parameters at the Eu site are presented in Sec. VI.

The intensity of the multiphonons of the B_{3u} mode increases extraordinarily (about 10 times; see the inset of Fig. 3) when the temperature decreases: The spectra of Figs. 1, 3, and 4 have been recorded exactly at the same conditions and with the same incident beam power. Only some kind of resonant process can explain such behavior. The observation of the luminescence wide band at 2.3 eV (Fig. 4) with a parallel behavior leads one to think that these two processes should be related. As we shall see later, on lowering the temperature the Co-O(2) distance decreases about 2%. This effect could induce a sufficient change in the crystal field on the Co^{2+} ions to make partially efficient transitions between the quasiatomic $3d$ cobalt electronic levels which leads to the observed luminescence band. The band gap of this material, whose conduction and valence bands are mainly due to oxygen $2p$ and Co $3d$ levels, respectively, is expected to be larger than the nickelates one, which is around 4 eV.[11,21] For that reason no interband transition is expected under our experimental conditions. We are inclined to think that the transitions are to and from (first absorption and later emission) these quasiatomic cobalt crystal-field $3d$ levels, which lay in the gap and which have very probably some O(2) orbitals mixture because of the very short Co-O(2) bonds parallel to the a axis of the chains. In that way, through the mixing between the Co $3d$ crystal-field levels and the O orbitals, we can understand the selective enhancement of the intensity of the B_{3u} phonon related to Co and apical O(2) movements.

V. TEMPERATURE DEPENDENCE OF THE STRUCTURE

It has been already pointed out that only the frequencies of phonons related to O(2) and Eu motions increase about 2% when the temperatures decreases from 300 to 80 K, while the O(1) phonons remain invariable. From a structural point of view, this fact can be explained by a contraction of the a axis when the temperature decreases, where as the b and c axes are nearly unchanged.

In order to check this point, EXAFS spectra at the Co K edge and Eu L_{III} edge were carried out. The available energy range for the Co K edge is unfortunately very short (about 340 eV), because of the presence of the L_I Eu edge. The energy range of the spectrum is not good enough to obtain reliable fits of the several Co-O(1), O(2), Eu, and Ba distances.

The Eu ion has seven oxygens as nearest neighbors at three different distances: Four of these are in the XY plane and the other three are in the YZ plane (Fig. 5). A decrease in the X axis means that only the four oxygens in the XY plane may change their Eu-O distance on cooling. The analysis of the EXAFS signal, in order to get the variation with the temperature of the distances of the neighbors around the absorbing atoms, has been done using the well-known expression:[22]

$$\chi(k) = \sum_j \frac{N_j}{kR_j^2} \exp(-2k^2\sigma_j^2)\exp\left(\frac{-\Gamma_j R_j}{k}\right) \times f_j(k) \sin[2kR_j + \Phi_j(k)] .$$

This equation describes the EXAFS oscillations for a Gaussian distribution of N_j atoms at mean distances R_j around the absorbing atom considering the single scattering and plane-wave approximation. **k** is the photoelectron wave vector, related to the electron mass (m_e) and with the threshold energy (E_0) by $k = [2m_e/\hbar^2(E -$

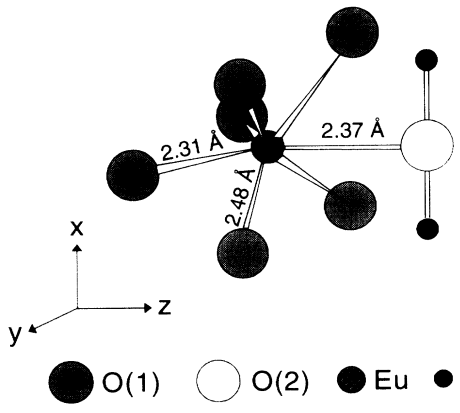

FIG. 5. Eu^{3+} environment in Eu_2BaCoO_5 with the $Immm$ structure with seven oxygen first neighbors and three different distances.

$E_0)]^{1/2}$; N_j is the average coordination number for the Gaussian distribution of distances centered at the R_j value, σ_j is the Debye-Waller contribution, and $\Phi_j(k) = 2\delta(k) + \gamma_j(k)$ is the phase shift, $\delta(k)$ and $\gamma_j(k)$ being the central and backscattering atom phase shifts, respectively. $f_j(k)$ is the magnitude of the backscattering amplitude of the jth-neighbor atom, and k/Γ_j is the mean free path of the photoelectron.

Figure 6 shows the Fourier transform of the EXAFS spectra at the Eu L_{III}-edge at RT and at the liquid nitrogen temperature (LNT). These functions are related to the radial distribution function around the absorbing atom, and the main peaks are related to the different coordination spheres of the Eu ions. The positions of the peaks must be corrected by the phase functions $\Phi_j(k)$ to obtain the true distances of the different coordination spheres in real space. We have taken the amplitude and phase functions reported by McKale *et al.*[23] The peak located at about 2 Å is related to the first oxygen coordination sphere and peaks centered at 3.0 Å and 3.6 Å are related to the Co, Eu, and Ba neighbors. The positions of these two peaks are compatible with the diffraction data, but no fine analysis can be performed because of the very similar distances (3.03, 3.66, and 3.94 Å, respectively) and the complexity of their backscattering amplitude functions.

Table III shows the EXAFS parameters that better fit the oxygen-related peaks. The RT values of the distances and coordination numbers have been taken as the ones given by x-ray-diffraction experiments.[24] The Debye-Waller, the mean free factor, and the energy shift have been fitted. The LNT parameters were obtained by fixing the shift and the Γ factor equal to the RT ones. In that way, the analysis gives that the distance to the four oxygens in the XY plane decreases while the other two Eu-O distances remain constant. This is consistent with the shortening only of the a axis at low temperature inferred from the frequency decrease observed in the Raman spectra.

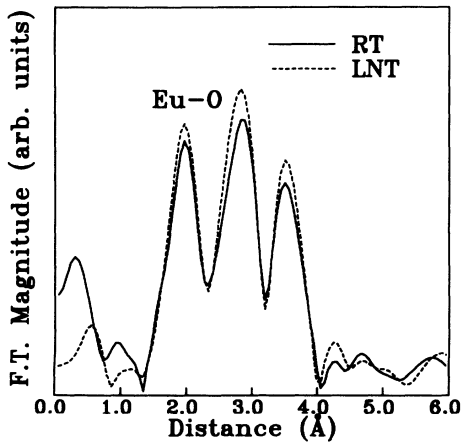

FIG. 6. Fourier transform of the EXAFS spectra at the Eu L_{III} edge at room temperature (RT) and at liquid nitrogen temperature (LNT).

TABLE III. EXAFS parameters of the best fit for the oxygen-related peaks at room temperature (RT) and liquid nitrogen temperature (LNT).

Temperature	Pair	R (Å)	N	σ (Å)	Γ (Å^{-2})	ΔE_0 (eV)
RT	Eu-O(1)	2.31	2	0.174	0.47	-14.0
	Eu-O(2)	2.37	1	0.053	0.47	
	Eu-O(1)	2.48	4	0.177	0.47	
LNT	Eu-O(1)	2.31	2	0.174	0.47	-14.0
	Eu-O(2)	2.37	1	0.053	0.47	
	Eu-O(1)	2.44	4	0.177	0.47	

VI. Eu^{3+} CRYSTAL-FIELD TRANSITIONS

The environment of the Eu ion is shown in Fig. 5, its local symmetry being C_{2v} with the twofold axis parallel to the Eu-O(2) bond (2.372 Å). One mirror plane contains this axis and two oxygen ions O(1) at 2.313 Å; the other plane is parallel to the paper. The four O(1), which are not on any symmetry element, are at the same distance from the Eu ion, at 2.481 Å. The different distances are indicated in Fig. 5.

The Eu^{3+} free-ion levels consist of a ^7F ground-state multiplet well separated from the excited states. The levels of the first excited ^5D multiplet are also far from any other level so that the mixing with other terms is not very important. Therefore, the assignment of the observed lines can be done keeping J as a good quantum number. The first excited level being $^5D_0$, the absorption to, or emission from, this singlet is sufficient to obtain the levels of the ground-state multiplet. These levels are the ones used to calculate the crystal-field parameters that describe the Eu^{3+} environment. Because of the C_{2v} local symmetry of the Eu ions, the degeneracy of the free-ion levels must be completely lifted so that $(2J + 1)$ levels are expected for each J term.

In Fig. 7 we present the emission spectra detected at 10 K and 300 K, in the spectral region between 13 000 cm^{-1} and 18 000 cm^{-1} (770 nm and 555.5 nm) when the excitation is achieved with three different lines of an Ar^+ laser (476.5, 488, and 514.5 nm). No emission peaks are detected between 18 000 cm^{-1} and 20 900 cm^{-1}. At room temperature, the peaks of Fig. 7 correspond to crystal-field transitions between $4f$ levels localized in the Eu^{3+} ions and are quite sharp as it corresponds to emissions between these kind of electronic levels (the width introduced by the experimental setup is around 5 cm^{-1}). The most intense peaks, around 16 000 cm^{-1}, are characteristic of the Eu^{3+} ion and correspond to the $^5D_0 \rightarrow {}^7F_2$ transitions. The assignment of the observed luminescence peaks has been done taking into account those done for Eu^{3+} in Y_2O_3 Ref. 26 and in $LiNbO_3$,[27] and based on the linewidths and the relative intensities of the observed peaks. Table IV summarizes the energies of the levels that can be deduced from the assignment of the observed lines.

Figure 8 shows the emissions from $^5D_0$ to $^7F_0$, $^7F_1$, and $^7F_2$, in detail at room temperature. In this figure the characteristic increase of the linewidth associated with the electron-phonon interaction is clearly observed.

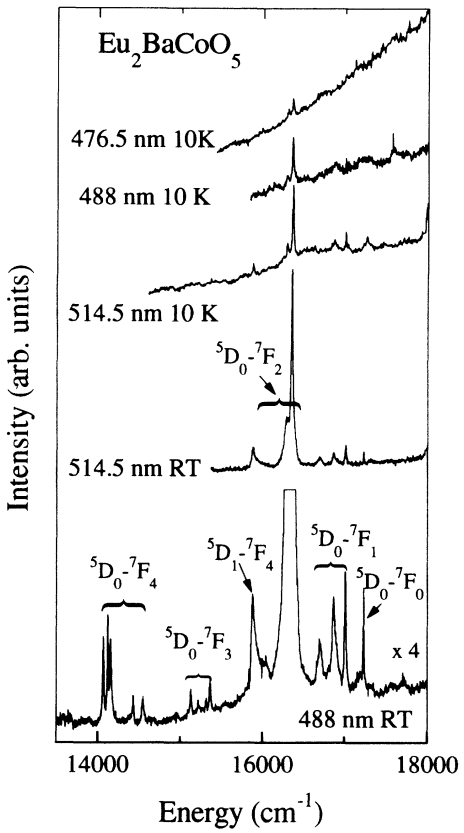

FIG. 7. Luminescence spectra of Eu_2BaCoO_5 at 300 and 10 K for three excitation wavelengths 476.5, 488, and 514.5 nm.

It is well known that the electronic transition from or to (corresponding to absorption or emission) the lowest crystal-field level of one term is the sharpest one and that the linewidth of the transitions to the other crystal-field levels of this term increases with the energy of the levels.[28] This is due to the possibility of relaxation to lower levels via spontaneous emission of phonons leading to a shorter lifetime of the higher-energy levels and a consequent broadening in energy. In Table V we present the parameters of the Lorentzian curves used to fit some experimental lines that show how the linewidth depends on the possibility of relaxation by phonons: The sharpest line corresponds to the transition $^5D_0 \rightarrow {}^7F_0$ where no relaxation of this kind is possible. The linewidth of transitions from the $^5D_0$ to the three levels of $^7F_1$ increases with the energy of these $^7F_1$ levels. The same behavior is observed in the transitions to the $^7F_2$ levels (only two peaks have been fitted, the other two being too weak). Therefore we have assigned the 15886 cm^{-1} peak to a $^5D_1 \rightarrow {}^7F_4$ transition rather than to a $^5D_0 \rightarrow {}^7F_2$ one because its linewidth (40 cm^{-1}) is much smaller than the expected one (more than 64 cm^{-1}).

A. Eu^{3+} crystal-field parameters

Although the complete scheme of the $4f^6$ configuration of Eu^{3+} has 3003 $|\alpha SLJM\rangle$ energy levels, the experimentally obtained set of energy levels seldom extends further than the ground-state multiplet ^7F and the first excited multiplet ^5D. This limited set of data is rarely sufficient to determine the large number of parameters (free ion and crystal field) necessary for a complete description of the Eu^{3+} ion inside a crystal. Nevertheless, because $4f$ electrons are only weakly perturbed by the crystal field, "free-ion" parameters introduced by the classical theories must be very similar to their free-ion values. So we can consider that the barycenters of ^7F_J and ^5D_J multiplets are only slightly deviated from their free-ion positions and we can use the spin-orbit and crystal-field terms as the more important ones in the Hamiltonian of Eu^{3+} inside a crystal structure. Moreover, it is well known that the levels of the first excited ^5D multiplet are very far from the ground-state multiplet (the $^7F_6$ — $^5D_0$ gap is usually larger than 10 000 cm^{-1}) and so the spin-orbit mixing between ^7F and ^5D levels is not very important. We can estimate that the ^7F wave functions have a predominantly pure ($\sim$ 95%) ^7F character, as in the free ion.[29] This fact allows a first attempt of crystal-field parametrization using, as restricted basis set, the

TABLE IV. Experimental and calculated values of the lowest terms of Eu^{3+} in Eu_2BaCoO_5.

Term (number of levels)	Level position (cm^{-1}) Experimental	Calculated
$^5D_1$	18700	—
(3)	(18930-54)	—
$^5D_0$	17263	—
	3168	3155
	3113	3125
	3078	3079
	2806	2817
$^7F_4$	—	2740
(9)	2691	2683
	2620	2617
	—	2447
	—	2351
	2106	2097
	2021	2018
	—	2009
$^7F_3$	1920	1926
(7)	1872	1874
	—	1812
	—	1738
	1240	1238
	1170	1165
$^7F_2$	951	966
(5)	881	872
	—	823
	526	542
$^7F_1$	364	363
(3)	221	208
$^7F_0$	0	0

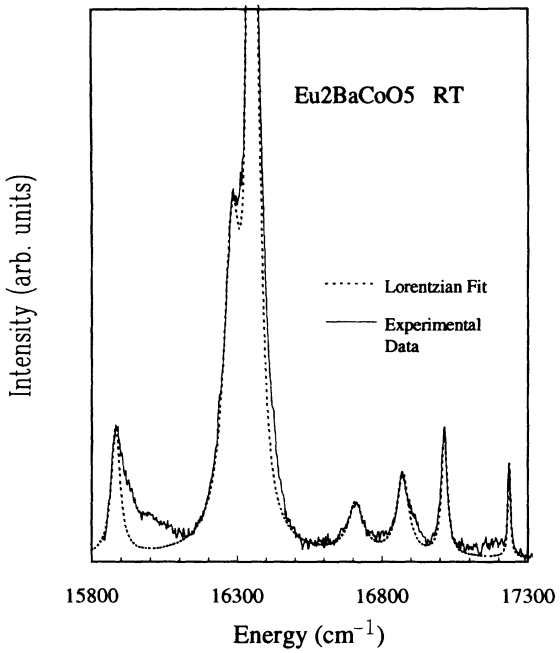

FIG. 8. Luminescence spectrum of the $^5D_0$ to $^7F_0$, $^7F_1$, and $^7F_2$ transitions at room temperature. The excitation wavelength is 488 nm.

pure LS-type eigenfunctions for the states of the ^7F multiplet.

For C_{2v} symmetry, the one-electron crystal-field Hamiltonian, can be written in the Wybourne form:[30]

$$\begin{aligned} H_{C_{2v}} &= B_2^0 C_0^{(2)} + B_2^2[C_{-2}^{(2)} + C_2^{(2)}] + B_4^0 C_0^{(4)} \\ &+ B_4^2[C_{-2}^{(4)} + C_2^{(4)}] + B_4^4[C_{-4}^{(4)} + C_4^{(4)}] + B_6^0 C_0^{(6)} \\ &+ B_6^2[C_{-2}^{(6)} + C_2^{(6)}] + B_6^4[C_{-4}^{(6)} + C_4^{(6)}] \\ &+ B_6^6[C_{-6}^{(6)} + C_6^{(6)}] , \end{aligned}$$

in which $C_q^{(k)}$ are the renormalized spherical harmonic tensors and B_k^q are the crystal-field parameters.

Initial estimates for the values of B_k^q parameters were obtained by direct calculation using the single point charge electrostatic model (PCEM), where all but the point charge effects (that is the covalent, multipole, exchange, etc.) are neglected. Because the Eu^{3+} ion is a constitutional ion (not an impurity), this static calculation appears as a quite good first approximation because no local distortion of the europium site is expected.

From the expression of the potential energy for the electrostatic interaction between the various atoms of the crystal lattice, the crystal-field parameters have the form

$$B_k^q = \langle r^k \rangle e^2 \left[\frac{4\pi}{2k+1}\frac{(k+q)!}{(k-q)!}\right]^{1/2} \times \sum_j \frac{g_j}{\rho_j^{k+1}} \frac{(1-x_j^2)^{-q/2}}{2^k k!} \frac{d^{k-q}(x_j^1-1)^k}{dx_j^{k-q}} e^{-iq\phi} ,$$

where g_j are the electric charges (in electron charge units), $x_j = \cos\theta_j$, and ρ_j, θ_j, ϕ_j are the polar coordinates of the atoms surrounding a rare earth atom selected as the origin.

Instead of the Hartree-Fock $\langle r^k \rangle_{\rm HF}$ mean radius values, we use the semiempirically corrected values $\langle r^k \rangle = \langle r^k \rangle_{\rm HF} (\frac{1-\sigma_k}{r^k})$, which include linear screening and scaling factors for rare-earth-ion wave functions into a solid.[31]

For PCEM calculation reference axes must be chosen so that all the B_k^q are real; we have selected a standardized axis set with the z axis along the twofold axis and x and y axes as shown in Fig. 5.[32] Convergent values of B_k^q obtained for PCEM calculations are shown in Table VI.

Using these *a priori* parameters, the experimental crystal-field parameters were obtained by diagonalizing the crystal-field Hamiltonian in the restricted LS basis and parameter refining with a least-squares method.

As pointed out previously, a zero-order approximation is carried out where LS-type eigenfunctions for the states of the ^7F_J ($J = 0, 1, ..., 6$) multiplet are considered for the fitting. Since each ^7F_J state is $(2J+1)$-fold degenerate, this approximation ends up with a 49×49 matrix, including full J mixing. In this truncated representation, the matrix elements of the $C_q^{(k)}$ tensors can be easily calculated from the Wigner-Eckart theorem using the tabulated values of fractional parentage coefficients[33] and Racah $3j$ and $6j$ symbols.[34]

Only the components of the ^7F_J levels with $J = 0, ..., 4$ are experimentally found, due to the weakness of the transitions to the $^7F_5$ and $^7F_6$. Out of the 49 ^7F_J components only 17 can be unambiguously derived from the

TABLE V. Parameters of the Lorentzian curves used to fit some of the observed transitions between Eu^{3+} $4f$ levels.

Transition	Energy (cm^{-1})	FWHM[a] (cm^{-1})	Integrated intensity (arb. units)
$^5D_0 \rightarrow {}^7F_0$	17236	10	325
	17016	20	930
$^5D_0 \rightarrow {}^7F_1$	16871	48	1330
	16710	60	1000
$^5D_0 \rightarrow {}^7F_2$	16257	32	14400
	16286	64	6240
$^5D_1 \rightarrow {}^7F_4$	15886	40	1800

[a]Full width at half maximum (FWHM).

TABLE VI. Crystal-field parameters (in cm^{-1}) of Eu^{3+} in Eu_2BaCoO_5.

	PCEM	Fitted values
B_2^0	-2383	-1266 ± 32
B_2^2	-561	-458 ± 11
B_4^0	-1153	-1464 ± 37
B_4^2	-2536	-2062 ± 27
B_4^4	1838	1482 ± 38
B_6^0	-417	-782 ± 19
B_6^2	-554	-519 ± 13
B_6^4	-523	-433 ± 11
B_6^6	-670	-591 ± 15

emission spectrum. This leads to the high uncertainty in the values of some crystal-field parameters. The fitted values of the crystal-field parameters are summarized in Table VI. Semiempirical values of the energy level positions, obtained using the experimentally fitted values, are shown in Table IV.

An inspection of Table VI reveals that PCEM parameters are very close to the fitted ones, mainly for nonaxial parameters, indicating that these electrostatic calculations are useful in order to obtain a good set of starting values for the real crystal-field parameters. The difference in the axial parameters can be explained taking into account two facts. First, PCEM B_2^0 overestimation, usually associated with short-range covalence effects on rank-2 parameters,[35] does not explain the coupled errors in the estimation of the other axial parameters B_4^0 and B_6^0. On the other hand, because the fitted crystal-field parameters are closer to their cubic values than PCEM values (this can be seen by using the cubic ratios), the axial parameters misfit must be interpreted as connected to a perturbation that reduces the axial character of the Eu^{3+} environment. Therefore it appears reasonable to associate the misfit in all axial parameters with strong covalence effects, mainly inside the chains formed by Co and apical oxygen O(2) with a very short bond distance.

B. Luminescence excitation processes

The behavior of the intensity of the luminescence peaks with temperature is, in principle, surprising: The intensity of the Eu^{3+} $4f$ transitions decreases drastically when the temperature is lowered (see Fig. 7). Indeed, only the strongest lines (around 16 000 cm^{-1}) are observed at 150 K but remain observable down to 10 K. On the other hand, the energies of the transitions are nearly independent of the temperature: An increase smaller than 3 cm^{-1} is detected when the temperature changes from 300 K to 10 K. This fact reveals that only small changes in the europium-oxygen distances occur. Nevertheless, it is well known that these $4f$ crystal-field transitions are not very sensitive to small variations in the distances, especially when the local symmetry is preserved.

Also notice that the intensity level is quite weak: For an excitation power of 10 mW, only around 1000 cps are detected. In fact no excitation or emission luminescence peaks are detected with a standard luminescence setup using a lamp and a photomultiplier in the current mode, probably in part because of the polycrystalline condition of the sample.

In the scheme of Fig. 9, the energies of the levels of some $4f$ terms are shown. The $^5D_1$ term is presented only as a grey zone because only one peak, corresponding to the emission to $^7F_4$ levels, is detected, and so the indetermination in energy is the width of this last term. The dashed heavy lines indicate the position in energy of the corresponding $^5D_1$ and $^5D_2$ levels of Eu^{3+}, in Y_2O_3;[26] their thicknesses correspond to the crystal-field splitting of each term in this compound. The dotted lines represent the positions of the three excitation beam energies (violet 20986, blue 20493, and green 19435 cm^{-1}) with

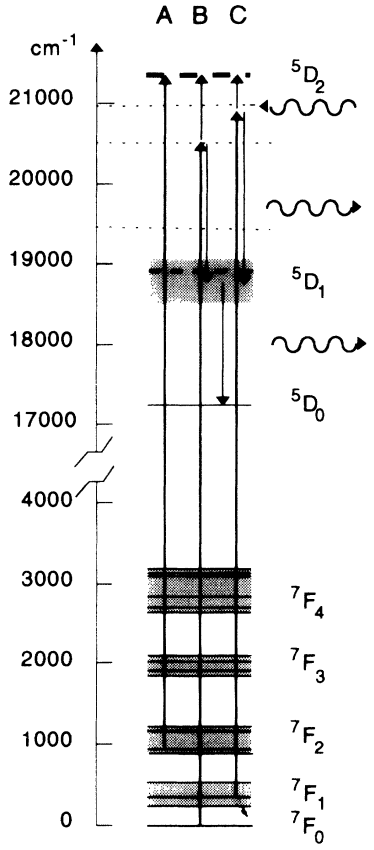

FIG. 9. Scheme of the lowest electronic levels in Eu^{3+} with the different proposed processes for the excitation (A, B and C). The arrows represent electronic transitions and the wavy arrows the phonons that are either absorbed or emitted. The dashed heavy lines are Eu^{3+} levels in Y_2O_3 and dotted lines represent the incident beam energies.

respect to the ground-state level ($^7F_0$) of the Eu^{3+} ion. None of the three excitation energies corresponds to an electronic transition from the ground state $^7F_0$; instead, the blue excitation coincides with the $^7F_2 \rightarrow {}^5D_2$ one (arrow labeled with A in Fig. 9). The other possible excitation processes are represented in Fig. 9 (B and C) as arrows and involve phonon mediation as emission or absorption of lattice phonons (represented as wavy arrows). The A process is possible whenever the temperature is high enough to have an appreciable population of electrons in the $^7F_2$ levels. While at room temperature this population is about 8×10^{-3}, at 150 K it is 120 times less and negligeable at 10 K, and so this process is not important at low temperatures. The B and C processes can either take phonons of the lattice to reach the $^5D_2$ levels or emit phonons to fall in the $^5D_1$ ones. Since the density of phonons present in the lattice decreases exponentially with the temperature, from the several excitation processes, only the B one, with relaxation to the $^5D_1$ term, is important at low temperatures.

The dependence of the emission with the incident wavelength is also seen in Fig. 7 in the spectra recorded at 10 K. The intensity of the Eu^{3+} luminescence peaks increases when the energy of the incident beam decreases;

the spectra have been corrected by the incident power. This is in accordance with the proposed processes for excitation. The B process is favored when the incident energy decreases because it is nearer to the $^7F_0 \rightarrow {}^5D_1$ transition energy and so, even at low temperature, the excitation is somewhat efficient.

To summarize, at room temperature, the excitation of the $4f$ electrons is achieved by the transition from thermaly populated levels ($^7F_2$, $^7F_1$); B and C processes also contribute. At low temperatures, only a transition to a virtual state with the emission of phonons is efficient (B process).

This kind of system is known to be charge transfer insulators with a band gap around 2 eV for cuprates and 4 eV for nickelates.[21] The valence band is formed with the $2p$ oxygen levels and the conduction one with the mixed $3d-4s$ transition-metal levels. The Ba empty levels are at much higher energies. The cobalt oxides are expected to have even a wider gap. In this compound, the Eu $^7F_0$ ground state, as well as all the excited $4f$ states described in this work, lie in the band gap. This kind of oxide presents a complicated electronic structure with band-type states, quasiatomic levels ($4f$ rare earth), and mixed-type ones (as the d levels of the transition metal). The simultaneous presence of these states around the gap and the importance of their relative position in energy is probably the reason for the different physical properties and effects on doping observed in related compounds which should be, in principle, similar.

VII. CONCLUSIONS

The comparison between the calculated eigenfunctions and frequencies of the optical normal modes and the observed phonons has allowed us to clarify the low-temperature Raman spectra of this compound. The temperature dependence of some infrared phonons, multiphonons, and electronic transitions is parallel, showing the interrelation between these two kinds of elementary excitations. The luminescence band (at 2.3 eV) is tentatively attributed to electronic transitions between Co^{2+} $3d$ crystal-field levels, in the gap of the material, partially mixed to apical oxygen [O(2)] orbitals along the chains. The mixing between Co and apical oxygen orbitals explains the simultaneous increase of the intensity of the luminescence band and that of the apical oxygen infrared modes through a resonance process. From the dependence of the phonon frequencies and the analysis of the EXAFS spectra with the temperature it can be concluded that the decrease of the temperature seems to shorten the a axis where as the other two axes are nearly unchanged.

The emission spectra of the Eu_2BaCoO_5 compound have been observed in the visible region at temperatures between 10 K and room temperature with three different excitation energies. The observed peaks at room temperature are associated with transitions between $4f$ localized levels of the Eu^{3+} ions of the sample. The scheme of the levels of this ion has been determined between 0 ($^7F_0$ ground state) and 19 000 cm^{-1} ($^5D_0$). The widths of the peaks related to transitions from the singlet $^5D_0$ to the ^7F_J levels (with J=0,1,2) show clearly the progressive broadening due to the shortening of the excited state lifetime because of the increase in the possibility of relaxation by spontaneous emission of phonons.

The crystal field acting on the europium ions has been evaluated using a simple electrostatic model, obtaining good agreement for the nonaxial crystal-field parameters. The axial parameters show some discrepancy which is related to the important covalent effects in the Co-O(2) chains (perpendicular to the z axis).

It has been shown that even using excitation energies quite far from a true electronic $4f$ transition it is possible to excite the luminescence via the coupling with optical phonons. The rapid decrease in the emission intensity when the temperature is lowered puts in evidence that, in our conditions, the main excitation processes are due to transitions from $^7F_1$ and $^7F_2$ multiplets which are only significantly populated at temperatures above 150 K and 200 K, respectively

ACKNOWLEDGMENTS

We thank R. Sáez-Puche and J. Hernández from Universidad Complutense de Madrid for the preparation of the samples used in this work. We thank also the CICyT for financial support under Project Nos. PB 92, 114-C04-04, and MAT93-793, and the LURE (Laboratoire pour l'Utilisation du Rayonnement Electromagnetique) for providing beam line time.

[1] J.A. Alonso, J. Amador, J.L. Martínez, I. Rasines, J. Rodríguez-Carvajal, and R. Sáez-Puche, Solid State Commun. **76**, 467 (1990).
[2] E. García-Matres, J.L. Martínez, J. Rodríguez-Carvajal, J.A. Alonso, A. Salinas-Sánchez, and R. Sáez-Puche, J. Solid State Chem. **103**, 322 (1993).
[3] J.K. Burdett and J.F. Mitchell, J. Am. Chem. Soc. **112**, 6571 (1990).
[4] A. de Andrés, J.L. Martínez, R. Sáez-Puche, and A. Salinas-Sánchez, Solid State Commun. **82**, 931 (1992).
[5] A. de Andrés, S. Taboada, J.L. Martínez, A. Salinas-Sánchez, J. Hernández, and R. Sáez-Puche, Phys. Rev. B **47**, 14898 (1993).
[6] Yu. A. Hadjiiskii, R.Z. Levitin, B.V. Mill, B.V. Paukov, M.N. Paupova, and V.V. Snegurev, Solid State Commum. **85**, 743 (1993).
[7] I. Paukov, M.N. Popova, and B.V. Mill, Phys. Lett. A **169**, 301 (1992).
[8] E.T. Heyen, W. Wegerer, E. Schönherr, and M. Cardona, Phys. Rev. B **44**, 10195 (1991).
[9] J. Lorenzana and L. Yu, Phys. Rev. Lett. **70**, 861 (1993).
[10] M. Shimida, M. Shimizu, J. Tanaka, I. Tanaka, and H. Kojima, Physica C **193**, 227 (1992).
[11] S. Tajima *et al.*, J. Opt. Soc. Am. B **6**, 475 (1989).

[12] C.H. Rüscher, M. Götte, B. Schmidt, C. Quitmann, and G. Güntherodt, Physica C **204**, 30 (1992).
[13] M. Yoshida, S. Tajima, N. Koshizuha, S. Tanaka, S. Uchida, and S. Ishibashi, Phys. Rev. B **44**, 11997 (1991).
[14] L. Terasaki, T. Nakahashi, A. Maeda, and K. Uchinikura, Phys. Rev. B **47**, 451 (1993).
[15] M. Born and K. Huang, *Dynamical Theory of Crystal Lattices* (Oxford University Press, Oxford, 1954).
[16] P.P. Ewald, Ann. Phys. (Leipzig) **64**, 253 (1921).
[17] T.L. Gilbert, J. Chem. Phys. **49**, 2640 (1968).
[18] M. Kunz and T. Armbruster, Acta Crystallogr. B **48**, 609 (1992).
[19] S.L. Chaplot and K.R. Rao, J. Phys. C **16**, 3045 (1983).
[20] B. Hu and R.S. Katiyar, Phys. Status Solidi B **174**, 375 (1992).
[21] S. Hüfner, P. Steiner, I. Sander, F. Reinert, and H. Schmitt, Z. Phys. B **86**, 207 (1992).
[22] B.K. Teo, *EXAFS: Basic Principles and Data Analysis*, Inorganic Chemistry Concepts Vol. 9 (Springer-Verlag, Berlin, 1986).
[23] A.G. McKale, B.W. Veal, A.P. Paulikas, S.K. Chan, and G.S. Knapp, J. Am. Chem. Soc. **110**, 3763 (1988).
[24] J. Hernández, A. Salinas, and R. Saéz-Puche, J. Solid State Chem. **110**, 321 (1994).
[25] Yu.A. Hadjiiskii, R.Z. Levitin, B.V. Mill, B.V. Paukov, M.N. Paupova, and V.V. Snegurev, Solid State Commun. **85**, 743 (1993).
[26] A.A. Kaminskii, *Laser Crystals*, Springer Series in Optical Sciences Vol. 14 (Springer-Verlag, Berlin, 1975).
[27] L. Arizmendi and J.M. Cabrera, Phys Rev. B **31**, 7187 (1985).
[28] S. Hüfner, *Optical Spectra of Transparent Rare Earth Compounds* (Academic Press, New York, 1978).
[29] G.S. Ofelt, J. Chem. Phys. **38**, 2171 (1963).
[30] R. G. Wybourne, *Spectroscopic Properties of Rare Earths* (Wiley, New York, 1965).
[31] C.A. Morrison and R.P. Leavit, J. Chem. Phys. **71**, 2366 (1979).
[32] Transformations of crystal-field parameters to this from other axis set can be made using the transformation rules given in C. Rudowicz and R. Bramley, J. Chem. Phys, **83**, 5192 (1985).
[33] I.I. Sobel'man, *An Introduction to the Theory of Atomic Spectra* (Pergamon, Oxford, 1972).
[34] Computer program MATHEMATICA, version 2.2, Wolfram Research Inc., 1993.
[35] H.J. Linburg, J. Hölsä, P. Porcher, G. Hergoz, D. Starick, and H. Wulff, Philos. Mag. B **67**, 541 (1993).

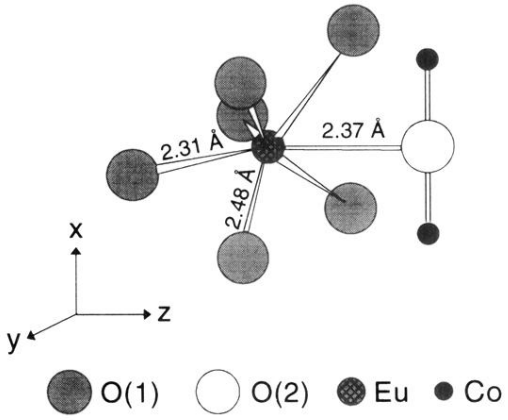

FIG. 5. Eu^{3+} environment in Eu_2BaCoO_5 with the $Immm$ structure with seven oxygen first neighbors and three different distances.

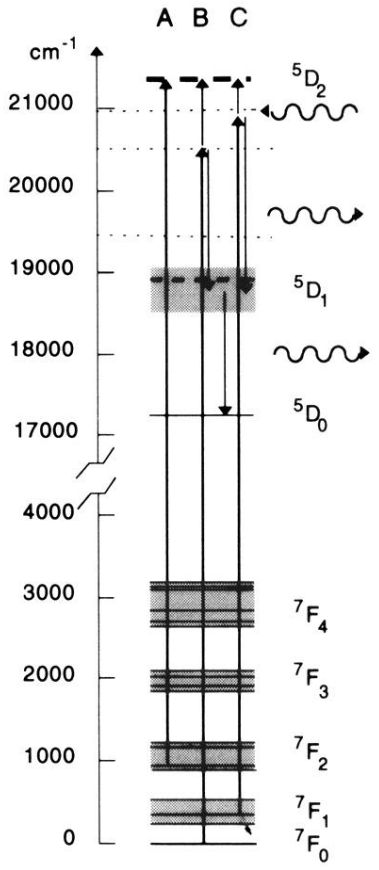

FIG. 9. Scheme of the lowest electronic levels in Eu^{3+} with the different proposed processes for the excitation (A, B and C). The arrows represent electronic transitions and the wavy arrows the phonons that are either absorbed or emitted. The dashed heavy lines are Eu^{3+} levels in Y_2O_3 and dotted lines represent the incident beam energies.